ICARUS 63, 272–289 (1985)

A Perturbative Treatment of Motion near the 3/1 Commensurability

JACK WISDOM

Department of Earth, Atmospheric, and Planetary Sciences, Massachusetts Institute of Technology, Cambridge, Massachusetts 02139

Received January 26, 1985; revised May 10, 1985

A semianalytic perturbation theory for motion near the 3/1 commensurability in the planar elliptic restricted three-body problem is presented. The predictions of the theory are in good agreement with the features found on numerically generated surfaces of section; a global understanding of the phase space is achieved. The unusual features of the motion discovered by J. Wisdom (1982, *Astron. J.* **87,** 577–593; 1983a, *Icarus* **56,** 51–74) are explained. The principal cause of the large chaotic zone near the 3/1 commensurability is identified, and a new criterion for the existence of large-scale chaotic behavior is presented.

I. INTRODUCTION

That there are gaps in the distribution of asteroids near low-order mean-motion commensurabilities with Jupiter was discovered in the last century, yet there is still no generally accepted explanation of their origin. A significant obstacle is that the long-term behavior of trajectories near commensurabilities in the elliptic-restricted three-body problem is not understood. There is no analytic theory for this motion and the numerical experiments have been too limited (by expense) to give significant insight. The numerical problems were largely overcome with the development of a new "mapping" method for studying the long-term behavior near commensurabilities that is approximately 1000 times faster than previously used methods (Wisdom, 1982). When followed with the mapping, trajectories near the 3/1 commensurability display some very curious behavior, viz, they may spend as much as a million years with eccentricities below 0.1, and then suddenly jump to eccentricities larger than 0.3. If this behavior were common the 3/1 Kirkwood gap could be swept clear by close encounters and collisions with Mars. I have shown that in fact such behavior is common and is characteristic of trajectories in a large chaotic zone near the 3/1 commensurability. When the effects of phase mixing are removed the boundary of the 3/1 Kirkwood gap is sharp and corresponds precisely to the boundary of the 3/1 chaotic zone, within the errors of the asteroid orbital elements. Furthermore, the essential features of this picture have been verified with conventional numerical integrations of the exact equations of motion. These features include the unusual behavior of the eccentricity and the existence and width of the chaotic zone. Thus the possibility that these unusual features are artifacts of the mapping approximation is ruled out (Wisdom, 1983a). Since the time scale for the removal of material on these trajectories is short compared to the age of the Solar System (Wetherill, 1975), the existence of the 3/1 Kirkwood gap is entirely explained by this mechanism. More recently, I have shown by direct numerical integration that chaotic trajectories can actually reach such large eccentricities that they cross Earth's orbit as well as the orbit of Mars (Wisdom, 1985). Thus this chaotic zone not only accounts for the 3/1 Kirkwood gap, but is probably the long sought route by which meteorites are transported from the asteroid belt to Earth (Wisdom, 1983b, 1985; Wetherill, 1985).

0019-1035/85 $3.00

While it is now known that there is a large and significant chaotic zone near the 3/1 commensurability, it is dissatisfying that there is still no analytic theory for this behavior. There are still many unanswered questions. Why does the chaotic zone have the shape it has? Why do chaotic trajectories seem to have a high-eccentricity mode and a low-eccentricity mode? Why does quasiperiodic libration lead to such large variations in eccentricity? Why do there appear to be three distinct zones of quasiperiodic libration on the representative plane [cf. Fig. 6 in Wisdom (1983a) and Fig. 4 in Murray and Fox (1984)]? What governs the limit to the eccentricity growth in the planar elliptic problem? In fact, why is there a chaotic zone at all? Is it due to the short-period terms in the disturbing function, the overlap of second-order resonances, or something more complicated? It is still an open question whether or not chaotic behavior played a role in the formation of the other Kirkwood gaps, but before the even more complicated dynamics of these resonances is challenged it seems wise to try to understand the dynamics of the 3/1 resonance more thoroughly and answer these lingering questions. That is the purpose of this paper.

Most "numerical integrations" in this paper use the mapping. It has already been adequately shown that the mapping compares well with the exact differential equations (Wisdom, 1983a; Murray and Fox, 1984). The goal here is not to further demonstrate this fact, but to understand the very complicated behavior which has been found. In the next section, I review some of the basic characteristics of the long-term motion near the 3/1 commensurability. In Section III, I describe the perturbative approach used in this paper, which involves the identification of two timescales in the long-period problem and the analytic solution of the motion on the shorter of these two time scales. The very-long-period behavior is computed in Section IV under the assumption that the action of the motion on the shorter time scale is adiabatically conserved. Section V compares the resulting solutions to numerically generated surfaces of section, and some qualitative features of the solutions are described. The principal cause of the chaotic behavior is identified in Section VI, and a simple new criterion for the existence of large-scale chaotic behavior is presented. The limitations of the approximations used in this paper are discussed in Section VII, and a summary is presented in Section VIII.

II. REVIEW OF THE QUALITATIVE BEHAVIOR

In traditional descriptions of the phenomenon of libration the resonant argument $\sigma = pl + q\tilde{\omega} - (p + q)l_J$ plays a central role. Here l is the mean longitude, $\tilde{\omega}$ is the longitude of perihelion, and p and q are integers. The subscript J refers to Jupiter. Near resonance σ varies slowly compared to the mean motions of the asteroid and Jupiter. Those terms in the disturbing function which contain σ produce large effects relative to the short-period terms whose contributions tend to average to zero. A good approximation to the motion is obtain by considering only those terms in the disturbing function which contain σ. This approach was introduced by Poincaré (1902). For the circular restricted problem the resulting system of equations is integrable, and an extra integral may be identified. It is customary to plot several trajectories with the same value of this extra integral together using e and σ as polar coordinates. Such plots of e and σ are often called Poincaré diagrams. While the figures in Section IV bear some superficial resemblance to Poincaré diagrams, it is important to keep in mind that they are in fact not related. In the elliptic restricted problem considered here, the Poincaré diagram is of limited usefulness. In the averaged circular problem near the 3/1 commensurability σ either librates about π or circulates, depending on the initial conditions. In the unaveraged circular problem there is in addition a small chaotic zone whenever an infinite period

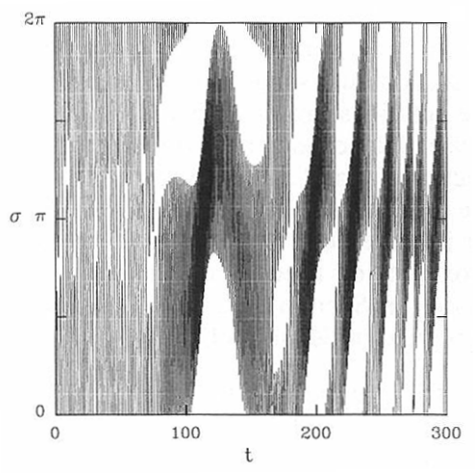

FIG. 1. The usual resonant argument $\sigma = l + 2\bar{\omega} - 3l_J$ versus time measured in millennia for a typical chaotic trajectory. This trajectory has $\Delta H = -4.22 \times 10^{-6}$.

trajectory separates libration from circulation (Chirikov, 1979; Wisdom, 1982, 1983a). The behavior of σ in the elliptic problem is much more complicated. An example of that behavior for a typical chaotic trajectory is shown in Fig. 1. Sometimes σ circulates and sometimes it librates. Sometimes it librates about a slowly varying center.

Figure 2 shows the eccentricity versus time for the same chaotic trajectory. It shows a transition from low-eccentricity behavior to high-eccentricity behavior. Typical chaotic trajectories show bursts of low-eccentricity behavior and bursts of high-eccentricity behavior. Each mode of behavior has apparently random duration, and has been observed to last from essentially no time at all (less than a few thousand years) to several million years. The behavior of the eccentricity is correlated with the behavior of the resonant argument, σ. During the low-eccentricity mode the resonant argument circulates or librates, but does not appear to be particularly coherent. On the other hand, during the high-eccentricity peaks, σ librates about a slowly varying center which goes through π when e is at a maximum.

The semimajor axis for this same trajectory is shown in Fig. 3. The behavior of the semimajor axis is also correlated with the resonant argument. During the high-eccentricity peaks the semimajor axis oscillates back and forth across the resonance zone. During the low-eccentricity mode the semimajor axis sometimes crosses the resonance center, but sometimes stays on only one side for a period of time. During those periods when the semimajor axis remains on one side of the resonance the resonant argument σ circulates. Thus short numeri-

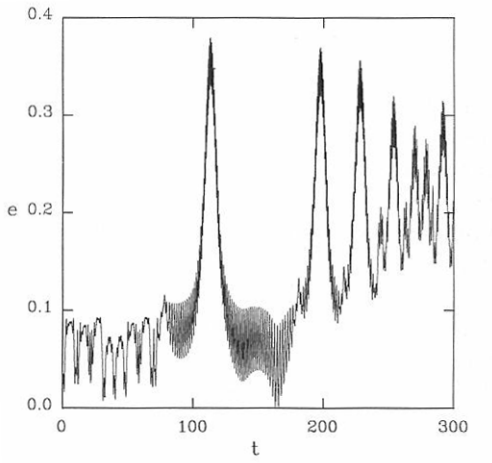

FIG. 2. The eccentricity versus time (in millennia) for the same trajectory as in Fig. 1.

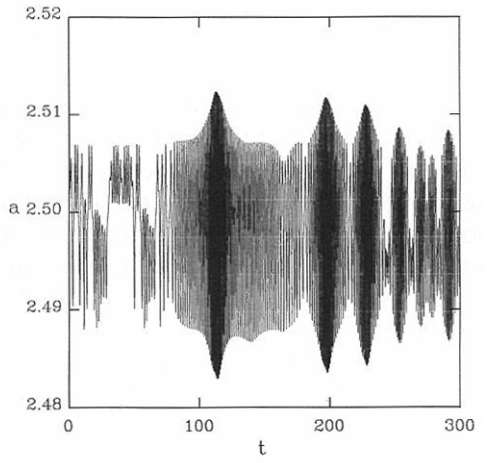

FIG. 3. The semimajor axis (in AU) versus time (in millennia) for the same trajectory as in Figs. 1 and 2.

cal integrations (less than 10,000 years) might identify the trajectory as a nonresonant, σ-circulating trajectory.

III. SOLUTION ON THE LIBRATION TIME SCALE

There are three natural time scales. The shortest time scale is the orbital period (a few years). The intermediate time scale is that of the libration of the resonant argument (typically a few hundred years). This time scale corresponds to the fastest oscillations visible in Figs. 1–3. The longest time scale is associated with the motion of the longitude of perihelion (typically several thousand years). This is the time scale for the slow evolution of the "guiding centers" of σ and e. The existence of several well-separated time scales could simplify the analytic treatment, especially if the fastest oscillations could be approximated analytically. In that case the longer period variations could be found by averaging the equations of motion over the fast oscillations, and, in turn, the changes in the solution for the fast oscillations could be found under the assumption that the action of the fast oscillations is adiabatically conserved during the slow evolution. Unfortunately, the latter two time scales are not always distinct. Nevertheless, in this section, I assume that the libration of the resonant argument is fast compared to the variation of the eccentricity and longitude of perihelion, and analytic approximations to the motion on the libration time scale are derived. Those situations where this assumption fails are identified in subsequent sections.

The resonant Hamiltonian for the planar-elliptic restricted three-body problem is (see Wisdom, 1982)

$$H = -\frac{\mu_1^2}{2L^2} - \mu R_{\rm sec}(\rho, \omega) - \mu R_{\rm res}(L, l, \rho, \omega),$$

where $R_{\rm sec}$ is the secular part of the disturbing function, $R_{\rm res}$ is the resonant part of the disturbing function, $\mu_1 = 1 - \mu$, and $\mu = 1/1047.355$ is the mass of Jupiter. Units are chosen such that $a_J = 1$ and $l_J = t$. In these units the period of Jupiter is 2π. The momenta L and ρ may be written in terms of the usual osculating elliptic elements: $L = \sqrt{\mu_1 a}$ and $\rho = \sqrt{\mu_1 a}\,[1 - (1 - e^2)^{1/2}]$, where a is the semimajor axis and e is the eccentricity. The conjugate coordinates are the mean longitude l and minus the longitude of perihelion ω, respectively. The disturbing functions are

$$R_{\rm sec} = -2\rho F - e_J G\sqrt{2\rho}\cos(\omega)$$

and

$$R_{\rm res} = 2\rho C\cos(l - 2\omega - 3l_J) + e_J D\sqrt{2\rho}\cos(l - \omega - 3l_J) + e_J^2 E\cos(l - 3l_J),$$

where those terms beyond second order in the eccentricity are ignored. The coefficients are evaluated at the resonant value of the semimajor axis and have the values $F = -0.2050694$, $G = 0.1987054$, $C = 0.8631579$, $D = -2.656407$, and $E = 0.3629536$. The eccentricity of Jupiter is given its current value $e_J = 0.048$. This Hamiltonian is a good representation of the dynamics near the 3/1 resonance.

The analytic development is considerably simplified if the difference of mean longitudes $\phi = l - 3l_J$ is used to describe the motion on the libration time scale rather than σ. Of course, ϕ and σ are essentially the same when the variation of ω is frozen. The momentum conjugate to ϕ is $\Phi = L$. At the same time it is convenient to change to the Poincaré momentum $x = \sqrt{2\rho}\cos(\omega)$ and its conjugate coordinate $y = \sqrt{2\rho}\sin(\omega)$. In these variables the Hamiltonian is

$$H = -\frac{\mu_1^2}{2\Phi^2} - 3\Phi + \mu F(x^2 + y^2) + e_J\mu Gx - \mu[C((x^2 - y^2) + e_J Dx + e_J^2 E]\cos\phi - \mu[C2xy + e_J Dy]\sin\phi. \quad (1)$$

Equivalently, this may be rewritten in the form

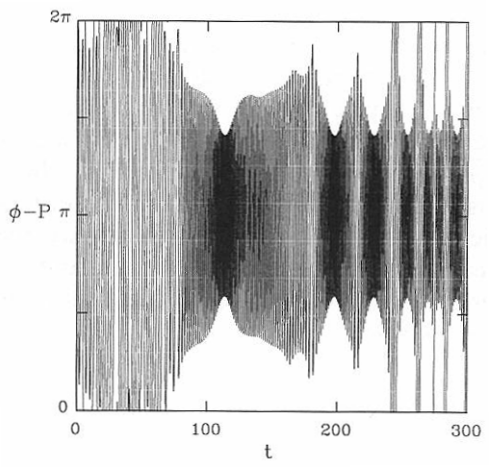

FIG. 4. The deviation of the angle $\phi = l - 3l_J$ from the guiding phase $P(x, y)$ versus time (in millennia) for the same trajectory as in Figs. 1–3. The slow drift has been removed, and $\phi - P(x, y)$ now circulates or librates with varying frequency and amplitude about π.

$$H = -\frac{\mu_1^2}{2\Phi^2} - 3\Phi + \mu F(x^2 + y^2) + e_J \mu G x - \mu A(x, y)\cos(\phi - P(x, y)), \quad (2)$$

where

$$A(x, y) = [(C(x^2 - y^2) + e_J D x + e_J^2 E)^2 + (2xyC + e_J D y)^2]^{1/2}$$

and

$$\tan P(x, y) = \frac{2xyC + e_J D y}{C(x^2 - y^2) + e_J D x + e_J^2 E}.$$

In this last form the "guiding center" of the ϕ libration is evident. To illustrate this Fig. 4 shows a plot of $\phi - P(x, y)$ for the same trajectory used in Fig. 1. There is no longer a slow drift, only a circulation or oscillation of varying amplitude and frequency about π.

At this point I assume that x and y are frozen, and may thus be treated merely as parameters in the equations of motion. Define $\lambda = \phi - P(x, y) - \pi$ and, in this approximation, its conjugate momentum $\Lambda = \Phi - \Phi_{res}$, where $\Phi_{res} = (\mu_1^2/3)^{1/3}$ is the center of the resonance defined by $\partial H/\partial\Phi = 0$. Expanding H about Φ_{res} and keeping only the quadratic terms, the Hamiltonian governing the variation of λ and Λ is

$$H' = \frac{1}{2}\alpha\Lambda^2 + \mu A \cos\lambda,$$

the ordinary pendulum Hamiltonian. It is helpful to keep in mind that the coefficient of the quadratic term $\alpha = -3\mu_1^2/\Phi_{res}^4 = -12.98851$ is negative.

The form of the solutions depends on the value of H': for $H' < -A$ the angle λ circulates, for $-A < H' < A$ the angle λ librates about zero, and the separatrix has $H' = -A$. The analytic solutions for the pendulum are well known, so I do not present their derivations. In the case of libration

$$\lambda = 4\sum_{n=1}^{\infty} \frac{\sin(2n-1)\omega t}{(2n-1)\cosh[(n - \frac{1}{2})\pi K'/K]},$$

where $K(k)$ and $K'(k)$ are the complete elliptic integrals of the first kind with modulus $k_L = ((\mu A - H')/2\mu A)^{1/2}$, and $\omega = \pi\omega_0/(2K)$. The frequency of small-amplitude oscillations is $\omega_0 = (-\alpha\mu A)^{1/2}$. The period of these small-amplitude oscillations depends on the eccentricity and longitude of perihelion through A, but is of order 150 years. The motion on the separatrix is

$$\lambda = 4\tan^{-1}(e^{-\omega_0 t}) - \pi.$$

In the case of circulation

$$\lambda = \omega t + 2\sum_{n=1}^{\infty} \frac{\sin n\omega t}{n\cosh(n\pi K'/K)},$$

with $\omega = \pi\omega_C/K$ and $\omega_C = (-\alpha(\mu A - H')/2)^{1/2}$. Here the elliptic modulus is $k_C = (2\mu A/(\mu A - H'))^{1/2}$. In each case the behavior of Λ may be determined through the relation $d\lambda/dt = \alpha\Lambda$. For completeness,

$$\Lambda = \frac{2\omega_0 k_L}{\alpha}\,\mathrm{cn}(\omega_0 t)$$

in the case of libration, and

$$\Lambda = \frac{2\omega_C}{\alpha}\,\mathrm{dn}(\omega_C t)$$

for circulation, where cn and dn are Jacobi

elliptic functions. The elliptic modulus for each case was given above. For circulation, an independent solution is obtained by multiplying λ and Λ by -1.

Several other properties of the pendulum are required in subsequent sections. For libration

$$\cos\lambda = 1 - 2k_L^2 \mathrm{sn}^2(\omega_0 t)$$

and

$$\sin\lambda = 2k_L \mathrm{sn}(\omega_0 t)(1 - k_L^2 \mathrm{sn}^2(\omega_0 t))^{1/2},$$

while for circulation

$$\cos\lambda = \mathrm{cn}^2(\omega_C t) - \mathrm{sn}^2(\omega_C t),$$

and

$$\sin\lambda = 2\mathrm{sn}(\omega_C t)\mathrm{cn}(\omega_C t),$$

where sn is another Jacobi elliptic function.

The action is defined by the integral.

$$I \equiv \frac{1}{2\pi}\oint \Lambda d\lambda.$$

The action is the libration case is

$$I = \frac{8}{\pi}\left|\frac{\mu A}{\alpha}\right|^{1/2}[E(k_L) - (1 - k_L^2)K(k_L)],$$

and the action in the circulation case is

$$I = \frac{4}{\pi}\left|\frac{\mu A}{\alpha}\right|^{1/2}\frac{E(k_C)}{k_C}.$$

$E(k)$ is the complete elliptic integral of the second kind.

IV. AVERAGING AND LONG-TERM EVOLUTION

Using Hamiltonian (2) the complete equations of motion are

$$\frac{dx}{dt} = -2\mu F y - \mu\frac{\partial A}{\partial y}\cos\lambda - \mu A\frac{\partial P}{\partial y}\sin\lambda,$$

$$\frac{dy}{dt} = 2\mu F x + e_J\mu G + \mu\frac{\partial A}{\partial x}\cos\lambda + \mu A\frac{\partial P}{\partial x}\sin\lambda,$$

$$\frac{d\lambda}{dt} = \frac{d\phi}{dt} - \frac{dP}{dt} = \alpha\Lambda - \frac{\partial P}{\partial x}\frac{dx}{dt} - \frac{\partial P}{\partial y}\frac{dy}{dt},$$

and

$$\frac{d\Lambda}{dt} = \frac{d\Phi}{dt} = \mu A\sin\lambda.$$

Since both dx/dt and dy/dt are proportional to μ the time scale for significant evolution of x and y is proportional to $1/\mu$. This is long compared to the period of small-amplitude oscillations of λ which is proportional to $\mu^{-1/2}$. Heuristically, only the average effect of the rapidly oscillating terms containing $\cos\lambda$ and $\sin\lambda$ will contribute to the large variations of x and y. This suggests that if x and y are divided into long-period parts and short-period parts, $x = \bar{x} + \xi$ and $y = \bar{y} + \eta$, the long-period variations may be determined from the equations

$$\frac{d\bar{x}}{dt} = -2\mu F\bar{y} - \mu\frac{\partial A(\bar{x},\bar{y})}{\partial\bar{y}}\langle\cos\lambda\rangle - \mu A(\bar{x},\bar{y})\frac{\partial P(\bar{x},\bar{y})}{\partial\bar{y}}\langle\sin\lambda\rangle$$

and

$$\frac{d\bar{y}}{dt} = 2\mu F\bar{x} + e_J\mu G + \mu\frac{\partial A(\bar{x},\bar{y})}{\partial\bar{x}}\langle\cos\lambda\rangle + \mu A(\bar{x},\bar{y})\frac{\partial P(\bar{x},\bar{y})}{\partial\bar{x}}\langle\sin\lambda\rangle,$$

where the angle brackets indicate an average over one oscillation period of λ. These averages are

$$\langle\cos\lambda\rangle \equiv \frac{1}{T}\int_0^T \cos\lambda dt = \frac{2E(k_L)}{K(k_L)} - 1$$

and

$$\langle\sin\lambda\rangle \equiv \frac{1}{T}\int_0^T \sin\lambda dt = 0,$$

for libration, and

$$\langle\cos\lambda\rangle \equiv \frac{1}{T}\int_0^T \cos\lambda dt = \frac{2E(k_C)}{k_C^2 K(k_C)} + 1 - \frac{2}{k_C^2}$$

and

$$\langle \sin \lambda \rangle \equiv \frac{1}{T} \int_0^T \sin \lambda dt = 0,$$

for circulation. In the evaluation of these expressions the table of integrals of squares of Jacobi elliptic functions in Abramowitz and Stegun (1970) is helpful.

The equations of motion for $\bar{x}$ and $\bar{y}$ are then

$$\frac{d\bar{x}}{dt} = -2\mu F\bar{y} - \mu \frac{\partial A}{\partial \bar{y}} \langle \cos \lambda \rangle \quad (3a)$$

$$\frac{d\bar{y}}{dt} = 2\mu F\bar{x} + \mu Ge_3 + \mu \frac{\partial A}{\partial \bar{x}} \langle \cos \lambda \rangle. \quad (3b)$$

Of course these equations are subject to the constraint that as $\bar{x}$ and $\bar{y}$ vary the elliptic modulus used in evaluating the expressions for $\langle \cos \lambda \rangle$ and $\langle \sin \lambda \rangle$ is chosen so that the appropriate action remains invariant. An alternate, more rigorous derivation of these equations is given in the appendix.

The advantage of the Poincaré diagram is that it gives at a glance a complete view of the motion for any given value of the extra integral. For the circular restricted problem that extra integral is just the Hamiltonian with all terms which do not involve σ removed by averaging. That Hamiltonian has only one degree of freedom. In the unaveraged circular problem, that "integral" exhibits short-period variations. However, it still restricts the motion and in many cases it is probably a first approximation to a true integral. I call such quantities "quasi-integrals." Hamiltonian (2) is the analogous quasi-integral for the elliptic restricted problem. This Hamiltonian has two degrees of freedom and is not integrable. The simplicity of the Poincaré diagram is thus lost. On the other hand, the fact that there are often two time scales allows much of this simplicity to be restored. The equations of motion for $\bar{x}$ and $\bar{y}$ are two dimensional, and must at least approximately conserve H. (It is not precisely conserved because of the adiabatic approximation and removal of the oscillations on the libration time scale.) It is possible then to plot a number of trajectories of $\bar{x}$ and $\bar{y}$ with (roughly) the same value of H to get a global view of the nature of such trajectories. In so far as the resulting trajectories all have the same value of the resonant Hamiltonian, the resulting plot is similar to the Poincaré diagram. Keep in mind though that the period of oscillation on the Poincaré diagram is the libration period, while here oscillations on the libration time scale have been removed by averaging to reveal a much longer period motion.

Examples of these plots $\bar{y}$ versus $\bar{x}$ for given values of H are shown in Figs. 5–7. These correspond, respectively, to curves 3–5 shown in Fig. 10 of Wisdom (1983a). When $\Lambda = 0$ the numerical values of H and H' differ by a constant term which was ignored in writing H'. That constant term is $\Delta = -3^{5/3}\mu_1^{2/3}/2$. Defining $\Delta H \equiv H - \Delta$, Figs. 5, 6, and 7 have $\Delta H = -1.21 \times 10^{-5}$, $\Delta H = -4.22 \times 10^{-6}$, and $\Delta H = -3.04 \times 10^{-6}$, respectively. Each trajectory is followed by an ordinary numerical integration of the equations of motion for $\bar{x}$ and $\bar{y}$ given above, subject to the constraint that the action for the λ motion keep its initial

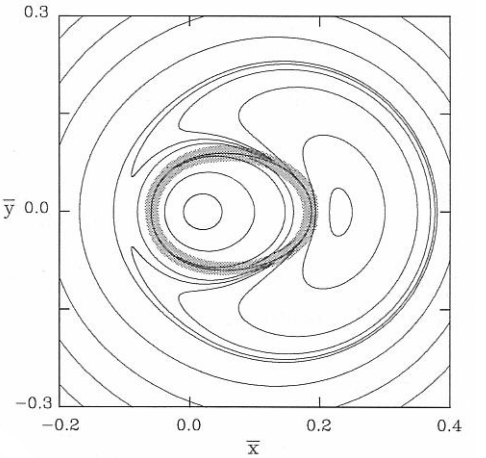

FIG. 5. The guiding trajectories in the $\bar{x}$, $\bar{y}$ plane for $\Delta H = -1.21 \times 10^{-5}$. The shaded region is the "zone of uncertainty," where the action of the λ oscillations is no longer conserved. λ circulates for guiding trajectories enclosed by the zone of uncertainty, and librates about π for all other trajectories.

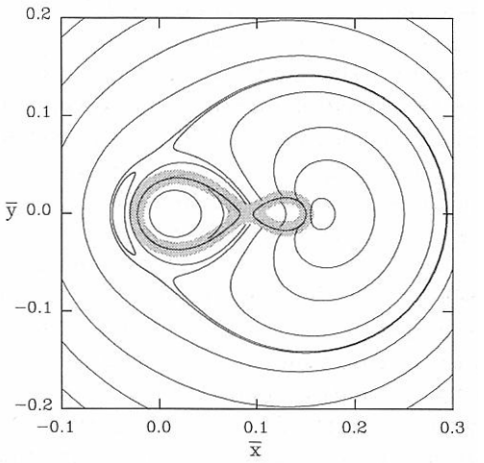

FIG. 6. The guiding trajectories for $\Delta H = -4.22 \times 10^{-6}$. The zone of uncertainty is again shaded, and has almost divided into two separate zones. λ circulates for guiding trajectories inside each lobe of the zone of uncertainty, and librates about π for all others.

value. The Bulirsch–Stoer algorithm with relative accuracy $\varepsilon = 10^{-11}$ was used to perform the integration.

Now, the assumption of adiabatic invariance of the action is only valid when the libration period is short compared to the periods associated with the variations of $\bar{x}$ and $\bar{y}$. Obviously, this assumption breaks down when the amplitude of oscillation of λ is near π, for then the pendulum period tends to infinity. In terms of the elliptic moduli, infinite periods occur when $k = 1$. This condition can be solved explicitly for the infinite period line $\bar{y}_\infty(\bar{x})$ for any given value of H. In particular, $k = 1$ occurs when $H' = -\mu A$. Substituting $H' = \Delta H - \mu F(\bar{x}^2 + \bar{y}^2) - \mu G e_1 \bar{x}$, and squaring both sides yields a quadratic equation for $\bar{y}_\infty^2$. The solutions of this equation are shown as lines in the middle of the shaded regions. It is clear that the approximation will also break down in some neighborhood of these curves as well. The shaded regions represent this neighborhood, but its actual extent remains undetermined. This region is called the "zone of uncertainty." It is in this zone that the actual trajectories can no longer be followed by the averaging method. The zone of uncertainty separates regions where λ oscillates from those where it circulates. In each case λ circulates in the region enclosed by the zone and librates in the region outside the zone. Trajectories follow a guiding trajectory until they reach the zone of uncertainty where they exhibit some complicated motions until finally they reappear on some neighboring guiding trajectory (with a different action) and the process is repeated.

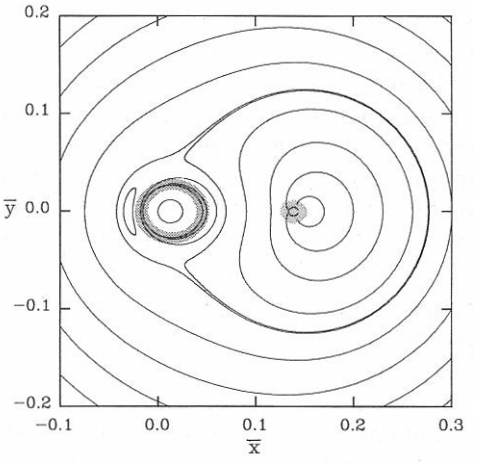

FIG. 7. The guiding trajectories for $\Delta H = -3.04 \times 10^{-6}$. The zone of uncertainty has now divided into two separate zones. Still, λ circulates for guiding trajectories inside each zone of uncertainty, and librates about π for all others.

An example of the actual appearance of a chaotic trajectory in the x, y plane is shown

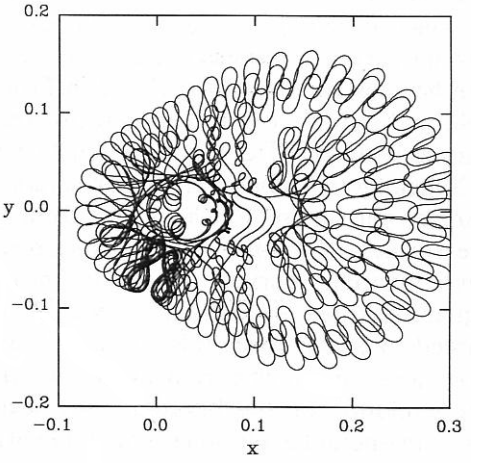

FIG. 8. The actual appearance in the $\bar{x}$, $\bar{y}$ plane of the chaotic trajectory represented in Figs. 1–4.

in Fig. 8. This is the same trajectory that was used in Figs. 1–4. However, the plot is complicated and the correspondence with the guiding trajectories (in particular Fig. 6) is not transparent. It is evident that an alternate method of comparison must be employed.

V. SURFACES OF SECTION

The fact that Hamiltonian (2) has only two degrees of freedom immediately suggests that it be studied with surfaces of section (see Hénon and Heiles, 1964). It is not, however, immediately apparent what the conditions for that section should be. One choice might be to plot x and y whenever $\Phi = \Phi_{\text{res}}$ (i.e., $a = a_{\text{res}}$), but I have illustrated how Φ avoids this value during much of the low-eccentricity mode. Another possibility is to plot x and y for some particular value of σ or ϕ, but Fig. 1 reveals that no choice of σ will adequately represent the high-eccentricity spikes. Giffen (1973) chose to plot a and σ versus e when a was at a maximum. Scholl and Froeschlé (1974, 1975, 1976, 1977, 1981) followed Giffen in this choice. This choice is satisfactory in that a regularly passes through a maximum during both the low-eccentricity mode and the high-eccentricity mode. However, two features make this choice unsatisfactory. First, a point on such a surface of section does not uniquely determine the trajectory to which it belongs. As a consequence invariant curves can cross one another! This can be seen by examining Fig. 2 in Froeschlé and Scholl (1976). The two invariant curves with initial eccentricities 0.18 and 0.20 belong to a family of similar invariant curves, yet the loops which they form on the surface of section are not concentric. Two invariant curves with more nearly equal starting eccentricities would be forced to cross. Also, this surface of section mixes the long-period evolution with the evolution on the libration time scale. The long-period evolution is not illuminated by such a plot. A much better choice would have been to plot the long-period variables x and y (or e and $\tilde{\omega}$) at every maximum or minimum of a. This section is similar to the section I use in this paper.

Figure 4 shows that ϕ regularly crosses its guiding center $P(x, y) + \pi$. To generate surfaces of section, I plot the canonically conjugate long-period variables x and y whenever $\phi - P(x, y)$ crosses π in a positive sense. This section removes the libration variable ϕ and its canonical momentum Φ. Points on the resulting surface of section are in one to one correspondence with trajectories which pierce the section. The perturbation analysis shows that this condition for section is almost the same as a passing through a minimum. For the numerical computations, I use the mapping. Strictly speaking the mapping differs from Hamiltonian (2) by short-period terms and possesses too many degrees of freedom to generate surfaces of section. However, this is also true of the planar-elliptic problem. In this sense the mapping is closer to the original problem than the averaged Hamiltonian, and in any case these short-period terms are largely unimportant. Computational economics dictates that I use the mapping. The typical length of the "integrations" used to produce the following surfaces of sections was 10^7 years per chaotic trajectory, an unpleasantly long time even for the numerical integration of the averaged Hamiltonian (2).

The surfaces of section for the three values of ΔH used in the last section are shown in Figs. 9–11. Because the mapping is not continuous in the time, I have plotted interpolated values of x and y for each crossing. The overall correspondance with the perturbation method is now evident. The two sets of figures do not quite superimpose because x and y are not equal to $\bar{x}$ and $\bar{y}$ when ϕ crosses $P + \pi$. The differences between these two sets of variables are computed in the appendix. The curves in Fig. 12 correspond to guiding trajectories in Fig. 6, but the correction from $\bar{x}$, $\bar{y}$ to x, y for $\phi = P + \pi$ has been applied. The structure of each plot is now identical. The agreement is excellent in the other two cases as well, though the curves become distorted if they

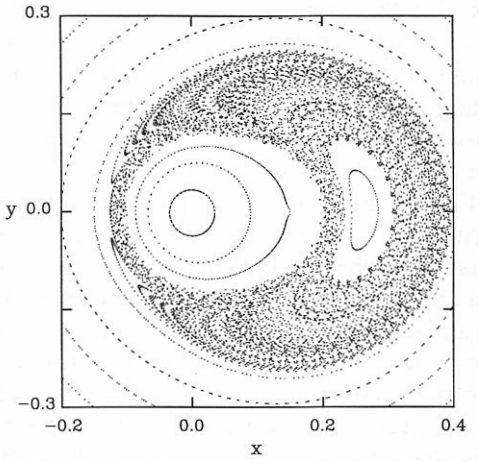

FIG. 9. Surface of section for $\Delta H = -1.21 \times 10^{-5}$. An interpolated point is plotted when ϕ crosses $P(x, y) + \pi$ in a positive sense. This figure corresponds to Fig. 5.

come too close to the points where $A = 0$ (see appendix). The quasiperiodic trajectories are well represented by the adiabatic approximation. This is also true of the chaotic trajectories when they are not near the zone of uncertainty. The chaotic zones are mainly filled with long arcs of dots which follow paths similar to those computed in Section IV. This behavior is most apparent in Fig. 9, which corresponds to Fig. 5.

Several qualitatively different types of quasiperiodic trajectories are present. In all the figures σ librates and $\bar{\omega}$ circulates on the outermost invariant curves, and both σ and $\bar{\omega}$ circulate on the invariant curves near the origin. In Figs. 9 and 11, there are quasiperiodic zones to the right of the quasiperiodic zone near the origin. In these quasiperiodic zones both σ and $\bar{\omega}$ librate (about π and 0, respectively). Finally, there are small islands to the left of the origin in Figs. 10 and 11, and here again both σ and $\bar{\omega}$ librate (about π). The existence of these island explains the appearance of several zones of quasiperiodic libration in Fig. 6 in Wisdom (1983a). All of these features are predicted by the perturbation analysis.

In Wisdom (1983a) the particular set of initial angles $\phi = \pi$ and $\bar{\omega} = \bar{\omega}_J = 0$ were conjectured to be representative of the phase space in the sense that almost all trajectories would eventually assume these angles. It is interesting to examine whether or not this conjecture is correct for the three surfaces of section. All of the quasiperiodic trajectories fill invariant curves which cross the x axis, and all but those in the small island to the left of the origin cross the positive x axis. When ϕ librates the guiding phase on this axis is such that it librates about either 0 or π. For x between $e_J(-D - \sqrt{D^2 - 4CE})/(2C) = 0.01$ and $e_J(-D + \sqrt{D^2 - 4CE})/(2C) = 0.14$ the guiding phase puts ϕ near zero when y is near 0, but outside this range ϕ librates about π near $y = 0$. Now consider the outermost invariant curves. These curves all cross the positive x axis ($\bar{\omega} = 0$) with ϕ librating near π. Since the libration frequency is in general incommensurate with the precession frequency the representative phases are approached arbitrarily closely. The innermost invariant curves also all cross the positive x axis, but this time ϕ circulates. Again, the generally incommensurate frequencies eventually give the representative angles. The same conclusion follows for the quasiperiodic zones to the right of the origin in Figs. 9 and 11, except that in Fig. 9 two representative crossings

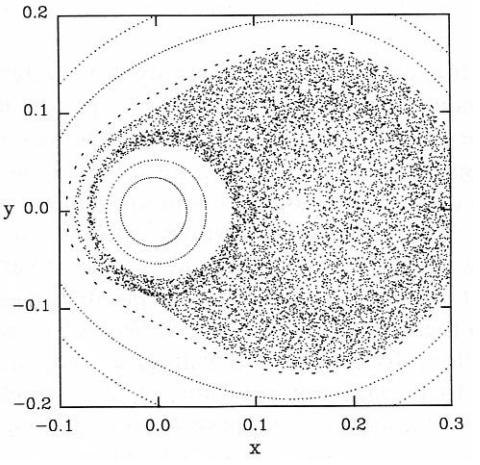

FIG. 10. Surface of section for $\Delta H = -4.22 \times 10^{-6}$. This figure corresponds to Fig. 6.

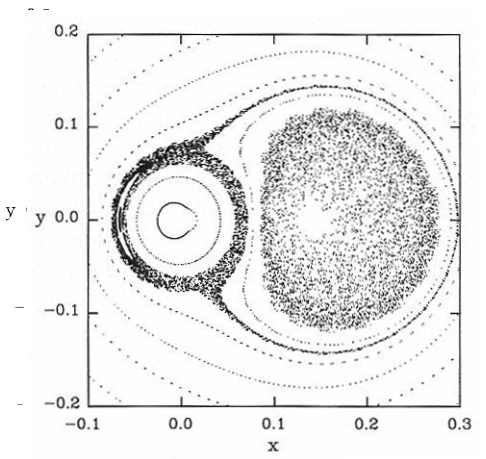

FIG. 11. Surface of section for $\Delta H = -3.04 \times 10^{-6}$. This figure corresponds to Fig. 7. There are two large chaotic zones for this value of ΔH. A trajectory in the chaotic zone surrounding the origin enters the narrow part of the chaotic zone which extends to high eccentricities at irregular intervals.

occur. (That this sometimes happens was noted in Wisdom (1983a).) It is obvious though that the small quasiperiodic zone to the left of the origin will never reach the representative angles, but this is evidently quite a small part of the phase space. While the representative plane is almost but not quite representative, as it happens the two planes of initial conditions presented in Wisdom (1983a) form complimentary pairs and are representative in the sense that almost all trajectories cross at least one of them.

It is possible now to identify the mysterious process whereby trajectories pass from the lower curves to the upper curves in Figs. 11 and 12 of Wisdom (1983a). Figure 10 corresponds to curve 4 in that paper. As a chaotic trajectory evolves in Fig. 10 it may spend some time near the inner invariant curves. During this time points appear on the lower part of curve 4. When the trajectory follows a (λ-librating) guiding trajectory to large eccentricity, points appear on the upper part of curve 4. Notice though that on Fig. 6 there is a small zone between the two zones of uncertainty where λ librates. For this zone ϕ librates about 0 near $y = 0$ and avoids values near π. Thus no points appear on the representative plane. There is a forbidden region on the representative plane, but on the surface of section the chaotic zone is continuous.

Finally, Fig. 11 makes clear the odd "intermittent" behavior shown in Fig. 13 of Wisdom (1983a). That trajectory belongs to the chaotic zone surrounding the origin. As described qualitatively in Wisdom (1983a) the chaotic zone has two parts: a low-eccentricity zone and a "narrow path to high eccentricity." As a trajectory wanders in this chaotic zone, it occasionally enters this narrow high-eccentricity path. It was observed that more generally there are two modes of behavior for a chaotic trajectory: a low-eccentricity mode and a high-eccentricity mode. These two modes correspond to different regions of the chaotic zone. In the low-eccentricty mode points appear around the quasiperiodic zone surrounding the origin. In the high-eccentricity mode points appear on the long arcs to the right side of the figures. The zone of uncertainty separates these two modes of behavior. Each time the trajectory emerges from this

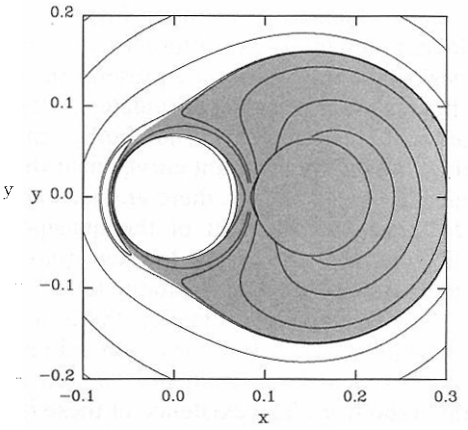

FIG. 12. Trajectories on the surface of section computed from the perturbation theory. These curves have $\Delta H = -4.22 \times 10^{-6}$, and correspond to Figs. 6 and 10. The region in which guiding trajectories terminate in the zone of uncertainty ($k > 0.99$) has been shaded.

zone it has a new λ action. Sometimes this action will place the trajectory in the low-eccentricity mode and sometimes in the high-eccentricity mode. (It should be explicitly mentioned that Fig. 11 shows two disjoint chaotic zones, one of which exhibits only the high-eccentricity mode.)

VI. ORIGIN OF THE CHAOTIC BEHAVIOR

One of the most useful criteria for predicting the onset of large-scale chaotic behavior is the resonance overlap criterion (see Chirikov, 1979). In this criterion, the location and widths of low-order resonances are analytically computed, and whenever the separation of two resonances is smaller than the sum of their half-widths a large zone of chaotic behavior is expected. This criterion is ideally suited to some problems. For example, the chaotic rotation of Hyperion was predicted using this criterion before it was verified numerically (Wisdom *et al.*, 1984). The resonance overlap criterion has also been used by Chirikov (1979) to determine the width of the chaotic separatrix in the presence of high-frequency perturbations. In other situations the application of the resonance overlap criterion is obscure, and it is not very useful. One example is the original problem of Hénon and Heiles (1964). Another is the problem considered in this paper! Now I have shown (Wisdom, 1980) that chaotic behavior does occur when resonances corresponding to different mean-motion commensurabilities overlap. Superficially, the problem of motion near the 3/1 commensurability looks quite similar (see Goldreich, 1982; Dermott and Murray, 1983). There is a large chaotic zone and at the same time there are three mean-motion resonances that strongly overlap. However, the fact that these resonances belong to the same commensurability is important. In this section, I show that the chaotic zone near the 3/1 commensurability is *not* a consequence of the overlap of these mean-motion resonances.

Near the 3/1 commensurability in the planar-elliptic problem the most important source of chaotic behavior seems to be associated with the zones of uncertainty. Comparison of Figs. 5–7 with Figs. 9–11 shows a close correspondence between the chaotic zones and the guiding trajectories which terminate near the zone of uncertainty. (The trajectories were terminated when $k > 0.99$.) This comparison for Figs. 6 and 10 is made explicit in Fig. 12. Trajectories on the surface of section for $\Delta H = -4.22 \times 10^{-6}$ have been computed using the correction from $\bar{x}, \bar{y}$ to x, y for $\phi = P + \pi$ derived in the appendix, and the region in which guiding trajectories terminate in the zone of uncertainty has been shaded. It is evident that a good prediction of the extent and shape of the chaotic zone can be obtained in this way.

Why is it that entering these zones of uncertainty leads to chaotic behavior? Away from them the action constitutes an approximate integral, and the trajectories behave predictably. Close to the zones of uncertainty the action is no longer conserved since the periods are not sufficiently different. However, the loss of the approximate integral is not in itself sufficient cause for chaotic behavior. As the trajectory enters the zone of uncertainty, the λ motion is forced near its separatrix, and motion near a separatrix is generally chaotic. It is possible that these temporary excursions into the chaotic λ separatrix are responsible for the large-scale chaotic behavior. The λ separatrix could become chaotic either as a result of the presence of the short-period terms in the disturbing function or the presence of the long-period evolution of the guiding trajectories. in the first case the chaotic behavior may be considered to result from the overlap of high-order resonances between the short-period terms and the much longer period λ oscillations near the separatrix (see Chirikov, 1979). In the latter case, as the period of the λ oscillations grows near the separatrix it must at some point become comparable to the periods associated with the $\bar{x}$, $\bar{y}$ motion. The

strengths of resonances between these two degrees of freedom grow as the periods become comparable and at some point resonances begin to overlap. The latter mechanism is undoubtedly more important, but to properly exhibit it the perturbation theory presented in the appendix would have to be carried further. The $\bar{x}$, $\bar{y}$ variables would themselves have to be converted to action-angle variables, and then the resonance structure analyzed for resonance overlap. Such an analysis should be able to predict the critical value of k above which the motion is chaotic. Of course, any guiding trajectories which terminate cross all values of k, so the actual critical value of k is irrelevant for them. To a first approximation the observed zones of chaotic behavior coincide with these terminating guiding trajectories. In Fig. 12, the shaded region corresponds to those guiding trajectories which reach $k > 0.99$. This choice was arbitrary. The actual critical value of k seems to be closer to 0.9. For this value all of the computed chaotic zones are in essentially exact agreement with the surfaces of section. In Fig. 12 the difference between these two critical values of k is slight, but with $k > 0.9$ the predicted chaotic zone surrounds the small island to the left of the figure as is observed in Fig. 10. While I have not demonstrated in terms of resonance overlap exactly why it happens, the fact remains that chaotic behavior seems to occur whenever, as a consequence of the adiabatic invariance of the action, the zone of uncertainty is entered.

It is desirable then to identify those features of the problem which lead to the crossing of the zone of uncertainty. That it is not a simple or necessary consequence of the overlap of mean-motion resonances may be demonstrated by considering the effect of removing the secular terms. The resulting problem still has three strongly overlapping mean-motion resonances, but trajectories, are no longer driven across the zone of uncertainty. This may be seen by considering Eqs. (3) with $F = G = 0$:

$$\frac{d\bar{x}}{dt} = -\mu \frac{\partial A}{\partial \bar{y}} \langle \cos \lambda \rangle$$

and

$$\frac{d\bar{y}}{dt} = \mu \frac{\partial A}{\partial \bar{x}} \langle \cos \lambda \rangle.$$

Since $\langle \cos \lambda \rangle$ depends only on A and some constants these equations are derivable from the Hamiltonian $\bar{H} = \bar{H}(A)$, where $\bar{H}(A)$ is defined by $d\bar{H}/dA = \mu \langle \cos \lambda \rangle$. Thus $A(\bar{x}\ \bar{y})$ is a constant of the guiding motion, and consequently so is the elliptic modulus. This means that to the extent that the action remains invariant the amplitude of the λ motion does not change and is never forced across its separatrix. There will thus be no large chaotic zone associated with trajectories forced to enter a zone of uncertainty. I have verified this by studying the surface of section for $\Delta H = -1.0 \times 10^{-5}$ with $F = G = 0$. The zone of uncertainty still exists and there is a small chaotic zone associated with it, but this zone is so small that it is barely visible on the scale of Figs. 9–11. There is no large chaotic zone when trajectories are no longer forced to enter the zone of uncertainty. I did not find chaotic zones near the unstable equilibria of the guiding trajectories, but I expect that with sufficient magnification this would be possible. However, such small chaotic zones are unimportant here. This example not only demonstrates the importance of entering the zone of uncertainty, but it shows that the broadened guiding separatrix is not an important source of chaotic behavior. (The width of the chaotic guiding separatrix is very small because the ratio of the libration frequency to the frequency of small-amplitude oscillations of $\bar{x}$, $\bar{y}$ is large and the width depends exponentially on this factor.)

The secular terms have been shown to be essential for large-scale chaotic behavior. I now show that in fact several overlapping resonant terms are not important. Consider first the circular problem, i.e., set $e_J = 0$. Hamiltonian (1) then contains a term pro-

portional to F and a resonant term proportional to C. In this case $A = C(x^2 + y^2)$. Since the secular part of the Hamiltonian is proportional to A, an argument similar to the one used in the last paragraph shows that A is a constant of the motion and the zone of uncertainty is not crossed. However, this crossing can be forced by adding an additional secular term. To illustrate this consider Hamiltonian (1) with $D = E = 0$ and $e_J = 0.5$. There is only one resonant term, but there are two secular terms. It is no longer true that the secular part of the Hamiltonian is proportional to A. Consequently, A is no longer a constant of the motion and many guiding trajectories are forced to terminate in the zone of uncertainty. A surface of section for this problem with $\Delta H = -1.0 \times 10^{-5}$ shows a large chaotic zone. The overlap of mean-motion resonances is a complicating factor, but not the cause of the chaotic behavior. The essential feature that gives rise to chaotic behavior is the crossing of the zone of uncertainty. For this to happen it is necessary that the secular Hamiltonian and A be independent of each other. It is not hard to show that in terms of Poisson brackets this condition for large-scale chaotic behavior may be stated $[R_{\text{sec}}, A] \neq 0$.

The overlap of mean-motion resonances is not responsible for the 3/1 chaotic zone. Rather, the chaotic zone arises because trajectories are forced to enter the zone of uncertainty.

VII. DISCUSSION

As a representation of the planar-elliptic restricted three-body problem, the most serious deficiency of Hamiltonian (1) is the truncation of the disturbing function to terms of order e^2. This neglects terms of order e^4. At large eccentricities the perturbation theory presented in this paper will be quantitatively incorrect. However, comparisons with ordinary numerical integrations show that it does a pretty good job even at eccentricities as high as 0.4 (Wisdom, 1983a; Murray and Fox, 1984). At much higher eccentricities the differences will become more serious and there will probably begin to be qualitative differences as well. At present these regions can only be studied numerically.

As a model for the motion of asteroids the planar-elliptic problem is itself deficient on two counts. It neglects the inclinations, and it neglects the long-period variations of Jupiter's orbital elements. The perturbation method I have presented in this paper can accomodate both of these complications. The shortest of the Solar System eigenperiods is 46,000 years (Brouwer and van Woerkom, 1950). Obviously the averaging over the libration time scale is still valid. The complicating factor is that the guiding trajectories can no longer be understood on a two-dimensional plot and can themselves be chaotic. Considering that the typical time scale for the precession of the perihelion is less than 20,000 years the Solar System secular variations may not have any major effect. (Remember though that in the inclined problem the "secular resonance" associated with this 46,000-year period approaches the 3/1 commensurability for "proper" inclinations near 15° (Williams and Faulkner, 1981). This shift in the position of the secular resonance with inclination depends on the mixed fourth-order terms in the secular disturbing function, i.e., terms of order e^2i^2.) Probably the more serious deficiency is the restriction to the plane. I have found that chaotic trajectories seem to exhibit more freedom in the three-dimensional restricted problem (reach higher eccentricities) and that the chaotic zone widens as the inclination to Jupiter's orbit plane increases (Wisdom, 1983a). There is no problem in carrying out the averaging for the three-dimensional problem, but now the averaged equations have two degrees of freedom. Thus again the guiding trajectories can themselves be chaotic. It may be the case that there are several chaotic zones, some associated with a zone of uncertainty and some associated with chaotic guiding trajectories. Perhaps the

proper context to understand the effects of the inclinations and the variations in Jupiter's orbital elements will be that of Arnold diffusion (see Chirikov, 1979).

VIII. SUMMARY

The general picture developed in this paper for motion near the 3/1 commensurability in the planar-elliptic restricted three-body problem is the following. Most of the time there exist three distinct time scales. Variations on the orbital time scale are generally ignorable. The libration time scale is usually so short compared to the precession time scale that analytic approximations for the variations on the libration time scale can be derived. With the assumption that the action of the libration motion is adiabatically preserved, the effect of the long-period evolution on the libration amplitude can be determined. In turn the variations on the libration time scale can be analytically averaged to obtain their effect on the long-period evolution of the eccentricity and longitude of perihelion. However, as a consequence of the preservation of the action the amplitude of the libration motion is sometimes driven near π, where the libration period becomes large. At this point the time scales are no longer distinct, and the action is no longer conserved. In this "zone of uncertainty" the analytic approximations can no longer be used to predict the motion. After some short time in the zone of uncertainty, trajectories reemerge to conserve some new value of the action until the zone of uncertainty is reached again. This picture of the motion is quite successful. It accurately predicts the "guiding centers" of σ and e, as well as numerous features of the surfaces of section. In particular the locations and shapes of the chaotic zones are accurately predicted by identifying chaotic trajectories with those guiding trajectories which are forced to enter the zone of uncertainty. That many trajectories are forced to enter the zone of uncertainty is recognized as the most important cause of chaotic behavior near the 3/1 commensurability in the planar-elliptic problem. The condition that this will happen takes the remarkably simple form $[R_{\text{sec}}, A] \neq 0$. I am not familiar with a simpler criterion for the existence of large-scale chaotic behavior.

Recently a number of authors (e.g., Torbett and Smoluchowski, 1982; Henrard and Lemaitre, 1983) have proposed cosmogonic theories to explain the existence of the Kirkwood gaps. Indeed, apart from its intrinsic interest as a classic problem in celestial mechanics, the primary goal in studying the distribution of asteroids is to understand more about how the Solar System formed, to place constraints on cosmogony. It is clear though that before this goal can be realized the dynamical mechanisms which could have modified that distribution over the billions of years since it was initially laid down must be properly understood. I have shown (Wisdom, 1982, 1983a) that in fact there exist important dynamical mechanisms for modifying the distribution of asteroids which were previously overlooked or discounted (Scholl and Froeschlé, 1974). In particular, the 3/1 commensurability is accompanied by a large chaotic zone, and trajectories within this chaotic zone cross planetary orbits. The existence and extent of the chaotic zone and the planet-crossing nature of the trajectories within it have been verified by conventional numerical integration (Wisdom, 1983a, 1985). The precise size and shape of the 3/1 Kirkwood gap is explained by the removal of the chaotic and quasiperiodic planet crossers. No cosmogonic mechanisms are required. This paper has presented a way of understanding why this chaotic zone is present and of predicting its general structure, at least in the planar-elliptic approximation. The general method will also work when the inclinations and secular variations of the planets are included, but a thorough investigation of the consequences is beyond the scope of this paper. Whether or not the inclinations and secular variations

introduce important qualitative changes in the dynamics (such as Arnold diffusion), quantitatively they are important in that trajectories in the 3/1 chaotic zone are Earth-crossing with them, but only Mars-crossing in the planar-elliptic approximation. The method presented in this paper should also work well for the other principal commensurabilities, to the extent that their dynamics are well represented by truncated disturbing functions. It seems that a good understanding of the long-term evolution of trajectories near commensurabilities in the Solar System is close at hand. Soon it may be possible to untangle those cosmogonic clues which lie dormant in the distribution of asteroids.

APPENDIX

This appendix presents an alternate derivation of Eqs. (3) using canonical perturbation theory. First, to prepare for the pendulum approximation a canonical transformation to the variables $\phi' = \phi$ and $\Phi' = \Phi - \Phi_{res}$ is made and only the quadratic terms in Φ' are kept. Since Φ' is of order $\mu^{1/2}$, this approximation ignores terms of order $\mu^{3/2}$. The next step is to transform the ϕ', Φ' variables to action-angle variables. This is accomplished by first solving the Hamilton–Jacobi equation for the pendulum

$$\Phi' = \frac{\partial F}{\partial \Phi'} = \pm\left\{\frac{2}{\alpha}\left[H' + \mu A \cos(\phi' - P)\right]\right\}^{1/2}$$

to obtain the generating function

$$F = \pm\int_{P+\pi}^{\phi'} \left\{\frac{2}{\alpha}\left[H' + \mu A \cos(\phi - P)\right]\right\}^{1/2} d\phi.$$

H' is considered to be a function of the action. Fortunately, the explicit inversion of $I(H', A)$ for $H'(I, A)$ can be avoided. The lower limit is chosen so that the angle conjugate to I is zero when $\phi' = P + \pi$. This integral could be evaluated in terms of elliptic integrals, but it is not required. The generating function for the full problem is then taken to be

$$F = -\int_{\bar{P}+\pi}^{\phi'} \left\{\frac{2}{\alpha}\left[\bar{H} + \mu\bar{A}\cos(\phi - \bar{P})\right]\right\}^{1/2} d\phi + x\bar{y},$$

where the identity transformation from x and y and $\bar{x}$ and $\bar{y}$ has been added, and H', $A(x, y)$ and $P(x, y)$ have been replaced by

$$\bar{H}(I, \bar{A}) = H'(I, A),$$
$$\bar{A}(x, \bar{y}) = A(x, y),$$

and

$$\bar{P}(x, \bar{y}) = P(x, y),$$

respectively. The minus sign is chosen so that $d\phi'/dt$ is positive when $\phi' = \bar{P} + \pi$. Since this generating function is time independent the new Hamiltonian is equal to the old Hamiltonian expressed in terms of the new variables. These new variables are obtained as derivatives of F:

$$\bar{x} = \frac{\partial F}{\partial \bar{y}} = x + \frac{\mu}{(-\mu\alpha\bar{A})^{1/2}}\left(\frac{\partial \bar{H}}{\partial \bar{A}}\frac{\partial \bar{A}}{\partial \bar{y}} I_1 + \frac{\partial \bar{A}}{\partial \bar{y}} I_2\right) + \Phi'(\phi')\frac{\partial \bar{P}}{\partial \bar{y}}$$

and

$$y = \frac{\partial F}{\partial x} = \bar{y} + \frac{\mu}{(-\mu\alpha\bar{A})^{1/2}}\left(\frac{\partial \bar{H}}{\partial \bar{A}}\frac{\partial \bar{A}}{\partial x} I_1 + \frac{\partial \bar{A}}{\partial x} I_2\right) + \Phi'(\phi')\frac{\partial \bar{P}}{\partial x}.$$

The two integrals in these expressions are

$$I_1 = \left(\frac{\mu\bar{A}}{-\alpha}\right)^{1/2} \int_{\bar{P}+\pi}^{\phi'} \frac{d\phi}{\left\{\frac{2}{\alpha}\left[\bar{H} + \mu\bar{A}\cos(\phi - \bar{P})\right]\right\}^{1/2}}$$

and

$$I_2 = \left(\frac{\mu\bar{A}}{-\alpha}\right)^{1/2} \int_{\bar{P}+\pi}^{\phi'} \frac{\cos(\phi - \bar{P})d\phi}{\left\{\frac{2}{\alpha}[\bar{H} + \mu\bar{A}\cos(\phi - \bar{P})]\right\}^{1/2}}.$$

For libration

$$I_1 = \mathrm{F}(\gamma, k_\mathrm{L})$$

and

$$I_2 = \mathrm{F}(\gamma, k_\mathrm{L}) - 2\mathrm{E}(\gamma, k_\mathrm{L}),$$

where $\mathrm{F}(\gamma, k_\mathrm{L})$ and $\mathrm{E}(\gamma, k_\mathrm{L})$ are elliptic integrals of the first and second kind, respectively, $\gamma = \sin^{-1}\{\mu\bar{A}[1 + \cos(\phi' - \bar{P})]/(\mu\bar{A} - \bar{H})\}$ and $k_\mathrm{L} = ((\mu\bar{A} - \bar{H})/(2\mu\bar{A}))^{1/2}$. The integrals have similar forms for circulation. The derivative $\partial\bar{H}/\partial\bar{A}$ is now determined by differentiating the formulae for the action with respect to $\bar{A}$. For libration

$$\frac{\partial\bar{H}(I, \bar{A})}{\partial\bar{A}} = \frac{2\mathrm{E}(k_\mathrm{L})}{\mathrm{K}(k_\mathrm{L})} - 1$$

and for circulation

$$\frac{\partial\bar{H}(I, \bar{A})}{\partial\bar{A}} = \frac{2\mathrm{E}(k_\mathrm{C})}{k_\mathrm{C}^2\mathrm{K}(k_\mathrm{C})} + 1 - \frac{2}{k_\mathrm{C}^2}.$$

Here $\mathrm{E}(k)$ and $\mathrm{K}(k)$ are complete elliptic integrals and the elliptic moduli are assumed to be written in terms of I and $\bar{A}(x, \bar{y})$. Collecting terms

$$\bar{x} = x + \frac{\mu}{\omega_0}\left[2E(k_\mathrm{L})\frac{F(\gamma, k_\mathrm{L})}{K(k_\mathrm{L})} - 2E(\gamma, k_\mathrm{L})\right]\frac{\partial\bar{A}}{\partial\bar{y}} + \Phi'(\phi')\frac{\partial\bar{P}}{\partial\bar{y}}$$

and

$$y = \bar{y} + \frac{\mu}{\omega_0}\left[2E(k_\mathrm{L})\frac{F(\gamma, k_\mathrm{L})}{K(k_\mathrm{L})} - 2E(\gamma, k_\mathrm{L})\right]\frac{\partial\bar{A}}{\partial\bar{y}} + \Phi'(\phi')\frac{\partial\bar{P}}{\partial\bar{x}},$$

for libration only.

The brackets containing elliptic functions are of order unity; Φ' is of order $\mu^{1/2}$; ω_0 is of order $e\mu^{1/2}$; $\bar{A}$ is of order e^2; derivatives of $\bar{A}$ are of order e. The derivatives of $\bar{P}$ are of order $e/\bar{A}$. Thus the two sets of variables seem to differ by terms of order $\mu^{1/2}$ as desired. However, each correction contains some power of $\bar{A}$ in the denominator, and while $\bar{A}$ is typically of order e^2 near (x, y) equal to $(0.01, 0)$ or $(0.14, 0)$ it is smaller. Denoting the distance in the x, y plane to these critical points by δ, the perturbation method breaks down when δ is less than a number of order $e\mu^{1/2}$. This restriction turns out not to be very serious. Such a restriction might have been expected on intuitive grounds. In the ordinary circular problem at large eccentricities the libration mechanism primarily involves the mean longitudes. On the other hand, at very low eccentricity the libration mechanism is mainly controlled by the motion of the perihelion. The approximation used here is more like the first case in that the variation of the mean longitudes is considered to dominate the motion on the libration time scale. It might be expected then that there would be regions where this assumption fails. It is perhaps surprising though that here there are two critical points, one at low eccentricity and one at moderate eccentricity ($x = 0.14$).

To order $e\mu^{1/2}/\delta$ the relation between the coordinates can be found by replacing $\bar{H}$, $\bar{A}$, and $\bar{P}$ by H', $A(\bar{x}, \bar{y})$, and $P(\bar{x}, \bar{y})$, respectively, in the expressions above. The explicit conversion from $\bar{x}$ and $\bar{y}$ to the surfaces of section is

$$x = \bar{x} + \left[\frac{2}{\alpha}(H' - \mu A)\right]^{1/2}\frac{\partial P}{\partial\bar{y}}$$

and

$$y = \bar{y} - \left[\frac{2}{\alpha}(H' - \mu A)\right]^{1/2}\frac{\partial P}{\partial\bar{x}}.$$

Finally, the new Hamiltonian is

$$H = H'(I, A(\bar{x}, \bar{y})) + \mu F(\bar{x}^2 + \bar{y}^2) + e_J\mu G\bar{x} + o(e\mu^{3/2}/\delta).$$

Since the angle conjugate to I does not appear, I is invariant to this order. The equa-

tions of motion for $\bar{x}$ and $\bar{y}$ are then

$$\frac{d\bar{x}}{dt} = -\frac{\partial H}{\partial \bar{y}} = -2\mu F\bar{y} - \frac{\partial H'}{\partial A}\frac{\partial A}{\partial \bar{y}}$$

and

$$\frac{d\bar{y}}{dt} = -\frac{\partial H}{\partial \bar{x}} = 2\mu F\bar{x} + e_J\mu G + \frac{\partial H'}{\partial A}\frac{\partial A}{\partial \bar{x}}$$

Since the expressions for $\partial H'/\partial A$ evaluated above are identical to the expressions for $\langle\cos\lambda\rangle$ evaluated in Section IV, these equations are the same as Eqs. (3).

ACKNOWLEDGMENTS

The basic approach of this paper, the separation of time scales and the use of the adiabatic invariance of the action to approximate the motion on the libration time scale, was suggested by Peter Goldreich. This work was supported in part by the NASA Planetary Geology and Geophysics Program under Grant NAGW 706.

REFERENCES

ABRAMOWITZ, M., AND I. A. STEGUN (1970). *Handbook of Mathematical Functions*. Dover, New York.

BROUWER, D., AND A. J. J. VAN WOERKOM (1950). *The Secular Variations of the Orbital Elements of the Principal Planets*. Astronomical Paper of the American Ephemeris XII, II.

CHIRIKOV, B. V. (1979). A universal instability of many dimensional oscillator systems. *Phys. Rep.* **52,** 263–379.

DERMOTT, S. F., AND C. D. MURRAY (1983). Nature of the Kirkwood gaps in the asteroid belt. *Nature* **301,** 201–205.

FROESCHLÉ, C., AND H. SCHOLL (1976). On the dynamical topology of the Kirkwood gaps. *Astron. Astrophys.* **48,** 389–393.

FROESCHLÉ, C., AND H. SCHOLL (1977). A qualitative comparison between the circular and elliptic Sun–Jupiter–asteroid problem at commensurabilities. *Astron. Astrophys.* **57,** 33–39.

FROESCHLÉ, C., AND H. SCHOLL (1981). The stochasticity of peculiar orbits in the 2/1 Kirkwood gap. *Astron. Astrophys.* **93,** 62–66.

GIFFEN, R. (1973). A study of commensurable motion in the asteroid belt. *Astron. Astrophys.* **23,** 387–403.

GOLDREICH, P. (1982). *Cosmology and Astrophysics (Essay in Honor of Thomas Gold)*, p. 121. Cornell Univ. Press, Ithaca, N.Y.

HÉNON, M., AND C. HEILES (1964). The applicability of the third integral of motion: Some numerical examples. *Astron. J.* **69,** 73–79.

HENRARD, J., AND A. LEMAITRE (1983). A mechanism of formation for the Kirkwood gaps. *Icarus* **55,** 482–494.

MURRAY, C. D., AND K. FOX (1984). Structure of the 3:1 Jovian resonance: A comparison of numerical methods. *Icarus* **59,** 221–233.

POINCARÉ, H. (1902). Sur les planetes du type d'Hecube. *Bull. Astron.* **19,** 289–310.

SCHOLL, H., AND C. FROESCHLÉ (1974). Asteroidal motion at the 3/1 commensurability. *Astron. Astrophys.* **33,** 455–458.

SCHOLL, H., AND C. FROESCHLÉ (1975). Asteroidal motion at the 5/2, 7/3 and 2/1 resonances. *Astron. Astrophys.* **42,** 457–463.

TORBETT, M., AND R. SMOLUCHOWSKI (1982). Motion of the Jovian commensurability resonances and the character of celestial mechanics in the asteroid zone: Implications for kinematics and structure. *Astron. Astrophys.* **110,** 43–49.

WETHERILL, G. W. (1975). Late heavy bombardment of the Moon and terrestrial planets. *Proc. Lunar Sci. Conf. 6th,* 1539–1561.

WETHERILL, G. W. (1985). Asteroidal source of ordinary chondrites. *Meteoritics* **18,** 1–22.

WILLIAMS, J. G., AND J. FAULKNER (1981). The positions of secular resonance surfaces. *Icarus* **46,** 390–399.

WISDOM, J. (1980). The resonance overlap criterion and the onset of stochastic behavior in the restricted three-body problem. *Astron. J.* **85,** 1122–1133.

WISDOM, J. (1982). The origin of the Kirkwood gaps: A mapping for asteroidal motion near the 3/1 commensurability. *Astron. J.* **87,** 577–593.

WISDOM, J. (1983a). Chaotic behavior and the origin of the 3/1 Kirkwood gap. *Icarus* **56,** 51–74.

WISDOM, J. (1983b). Chaotic behavior near the 3/1 commensurability as a source of Earth crossing asteroids and meteorites. *Meteoritics* **18,** 422–423.

WISDOM, J. (1985). Meteorites may follow a chaotic route to Earth. *Nature* **315,** 731–733.

WISDOM, J., S. J. PEALE, AND F. MIGNARD (1984). The chaotic rotation of Hyperion. *Icarus* **58,** 137–152.